Discrete-Time State-Space Construction Method for SSO Analysis of Renewable Power Generation Integrated AC/DC Hybrid System

Yingsheng Han, Haishun Sun, Biyue Huang, Shiyao Qin, Qing Mu, and Yongjun Yu

***Abstract*—Construction of the linearized state-space model is the key step of eigenvalue analysis for SSO study of power systems with large-scale renewable power generation (RPG) integrated. This paper proposes a novel method to construct the state matrix of the AC/DC hybrid power system with RPG within the discrete-time domain. The continuous-time state-space model of each AC/DC component as well as RPG units in the power system, is discretized together with their corresponding control. The discretized equation of each component is then represented by an equivalent circuit consisting of parallel historical current and conductance. According to the power system configuration, the discrete-time equivalent circuit of the whole AC/DC hybrid system is established, and the nodal analysis method is applied for the construction of the discrete-time state-space model of the power system. In this way, the state matrix can be acquired much more conveniently than that of continuous-time state-space method, which needs topology analysis to find independent state variables of the network from the proper tree. The proposed method has been applied in the eigenvalue analysis for the SSO study of a case system adapted from the AC/DC hybrid transmission system in northwest China. Eigenvalue results are in high accordance with time-domain simulation results in PSCAD/EMTDC.**

***Index Terms*—Subsynchronous oscillation, eigenvalue analysis, discrete-time state-space model (DSSM), discrete-time equivalent circuit model (DECM), AC/DC hybrid system, nodal analysis.**

I. Introduction

SUBSYNCHRONOUS oscillation (SSO) has always been an important issue that jeopardizes the secure and stable operation of the power system, especially in the case of large-scale renewable power generation integrated into the grid in recent decades [1]–[3]. In the traditional power system with synchronous generators as the primary source, the mechanism of SSO caused by the interaction between the generator shaft system and the series capacitor in AC lines or the control of high voltage direct current (HVDC) transmission has been clearly understood after several years of research [4]–[5]. However, with the rapid development of renewable power generation and voltage source converter (VSC)-based HVDC technologies [6]–[8], a new type of SSO problem induced by controls of power converters has occurred many times worldwide [9]–[13]. These typical oscillation incidents mainly occurred in the wind farms located in Texas of USA [9]–[10], Guyuan [12], and Hami [11] of China, where a large amount of wind power is sent out through series-compensated lines or directly integrated into a weak AC grid [14]–[16]. Besides, as the representative of wind farms connected via VSC-HVDC, the offshore wind plant in Nan'ao, China has also experienced SSOs [17]. Thus, it is of great significance to study the small-signal stability of the converter-based power systems, which will be the objective of this paper.

Significant efforts have been devoted to the dynamic stability of systems containing renewable power generations and VSC-HVDC [18]–[22]. It is found that the grid-side controller of wind farms or the inverter-side controller of VSC-HVDC may interact with the weak AC network, thus causing unstable SSO [6], [23]–[24] In addition, interactions between the controllers of the close electrical distance-connected converters may also result in instability of the system [25], such as the interaction between the grid-side controller of wind farms and the rectifier-side controller of the VSC-HVDC [18]. Nevertheless, the oscillation mechanism of the converter-based power systems needs to be further explored.

This paper mainly focuses on the SSO analysis method. Among the existing research works, the eigenvalue method [26]–[28], impedance method [29]–[30], and time-domain simulation method [31]–[32] are the three most often used analysis methods. The open-loop modal method [33] and the amplitude-phase dynamics method [34] are also developed in recent years to analyze the small-signal stability of power systems. Generally, the time-domain simulation method is used to validate the theoretical analysis results of other methods. Sometimes, the scale of the system simulated is limited, especially when the power electronic conversion devices are widely employed. Although the impedance method can explain the reason for SSO from the

Manuscript received April 23, 2021; revised July 22, 2021; accepted September 12, 2021. Date of publication September 24, 2021; date of current version April 19, 2022. This work was supported in part by the National Key Research and Development Program of China under Grant 2018YFB0904000 and in part by the Science and Technology Project of State Grid under Grant SGJB0000TKJS1801242. Paper no. TPWRS-00632-2021. *(Corresponding author: Haishun Sun.)*

Yingsheng Han, Haishun Sun, and Biyue Huang are with the State Key Laboratory of Advanced Electromagnetic Engineering and Technology, Huazhong University of Science and Technology, Wuhan, Hubei 430074, China (e-mail: hust_hanys@hust.edu.cn; haishunsun@hust.edu.cn; biyuehuang@hust.edu.cn).

Shiyao Qin and Qing Mu are with the China Electric Power Research Institute, Beijing 100192, China (e-mail: qinsyao@126.com; abel.qing.mu@outlook.com).

Yongjun Yu is with the State Grid Xinjiang Electric Power Research Institute, Urumqi 830011, China (e-mail: yujyuj@vip.sina.com).

Color versions of one or more figures in this article are available at https://doi.org/10.1109/TPWRS.2021.3115248.

Digital Object Identifier 10.1109/TPWRS.2021.3115248

perspective of circuit resonance [20], [35], it is hard to locate the dynamic parts strongly related to the dominant oscillation mode. The eigenvalue method can provide information such as eigenvalues and participation factors by linearizing the state equations and obtaining the state matrix, making it useful in SSO analysis and controller design [6], [26]. However, this method is limited by the system size and structure and is only used in simple systems at present. The open-loop modal method is based on the modal analysis of two open-loop subsystems. It can investigate the interaction between two subsystems but cannot clearly reflect the dynamic interaction of state variables within the subsystem [36]. The works in [37] prove the equivalence of the amplitude-phase dynamics method and the impedance method in analyzing the SSO stability of the converter-based power systems.

In brief, the above various SSO analysis methods have their own advantages and disadvantages in different application scenarios and cannot be generalized. This paper focuses on the eigenvalue method and is committed to solving its application limitations in large-scale power systems. Generally, the application of the eigenvalue analysis method in complex systems mainly faces modeling issues first. There are two tasks for modeling: 1) establishing the state-space model of each component suitable for SSO analysis; 2) building the whole system's state-space model including all components and obtaining the state matrix. The first task seems to be easy since, for most power system components, their accurate state-space models can be developed according to their operating characteristics or transfer functions. As for the second task, it may have some difficulties mainly because of the determination of independent state variables for state-space construction of the network, which might be improper topologically.

In the previous work for the state-space construction of a large system that may contain improper networks, the topology analysis is performed to obtain the proper tree at first [38]–[39]. Then, voltages across the capacitor tree-branch and currents in the inductor link-branch are selected as the independent state variables [39]–[41]. Finally, the network state-space model is acquired by eliminating the other intermediate variables through Kirchhoff's current law (KCL) and Kirchhoff's voltage law (KVL) [40]. This process is very complicated and inefficient, and it has to be repeated when the system structure is changed.

In the field of control theory, the eigenvalues of the system have a clear mapping relationship in the continuous-time and discrete-time domain, so it is also reasonable to conduct modal analysis within the discrete-time domain [42]. However, the existing general discrete-time state-space method in textbooks is to discretize the *full-order* continuous-time state-space model of the target system. Therefore, it has the same drawbacks as the continuous-time method in constructing the state matrix.

Literature [43] first proposed the idea of directly establishing the state-space model of electrical circuits based on the electromagnetic transients program (EMTP) solutions in the discrete-time domain. In this way, it did not require topology analysis on the improper network to find independent state variables. However, the works in [43] did not introduce the discrete-time models of complex power components, such as wind turbines and HVDC with their control parts included; on the other hand, it did not address the application of this method in the SSO analysis of large-scale converter-based power systems especially including RPGs and HVDC. Most importantly, the essential reasons for the advantages of constructing state-space models in the discrete-time domain were not explained.

This paper aims to resolve the above difficulties and extends the idea in [43] to the application of SSO analysis of complex AC/DC hybrid systems. Compared with the existing works, the main theoretical contributions of this paper are as follows:

1) This paper classifies the dynamic components of AC/DC power system into three categories and develops their discrete-time state-space models (DSSMs) and discrete-time equivalent circuit models (DECMs) respectively; the components within the same category have the same general form of discrete-time models;
2) This paper proves the proper characteristics of the discrete-time equivalent circuit network and the independence of all discrete-time state variables, providing the theoretical basis for the state-space construction within the discrete-time domain;
3) This paper proposes the discrete-time state-space construction method for AC/DC hybrid power systems using the nodal method, which is appropriate for large-scale converter-based power system dynamic stability analysis such as SSO; this method makes the state matrix of systems easy to be formed and modified under system structure changes.

The rest of the paper is organized as follows. Section II briefly introduces the related concepts of discrete-time eigenvalue analysis methods. Section III presents in detail the DSSMs and DECMs of various power system components. The algorithm for AC/DC hybrid system state-space construction is given in Section IV. Case studies for the SSO analysis using the proposed method are conducted in Section V, and the time-domain simulation results are presented in this section as well. Section VI gives some discussions on the advantages of the proposed method. Brief conclusions are drawn in Section VII.

II. Basic Concepts of the Discrete-time Eigenvalue Analysis Method

According to control theory, a linear time-invariant system (LTIS) can be described either by a set of linearized differential equations as (1) or difference equations as (2). Both of them are called the state-space equations of the system.

$$[\dot{X}] = [A_c][X] + [B_c][u] \tag{1}$$

$$[X(t+\Delta t)] = [A_d][X(t)] + [B_d][u(t)] \tag{2}$$

In the above equations, [*X*] is the variation of the state vector, [*u*] is the variation of the input vector, [*A*] is the state matrix, [*B*] is the input matrix. The subscript '*c*' and '*d*' denotes the continuous-time and discrete-time domain, respectively.

Without considering the forcing function ($u = 0$), the specific relationship of state matrix in different domains can be obtained as (3) by discretizing (1) with trapezoidal integration rule and

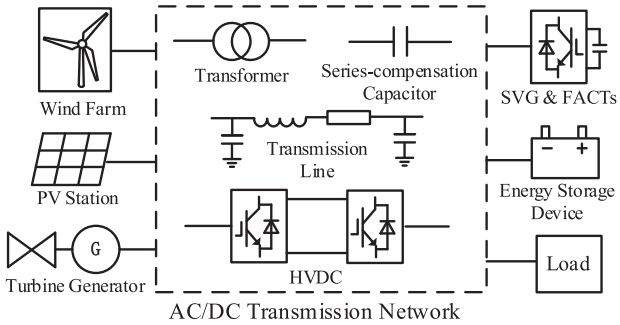

Fig. 1. A conceptual AC/DC hybrid system.

compared with (2):

$$[A_d] = (2[I] - \Delta t \cdot [A_c])^{-1} (2[I] + \Delta t \cdot [A_c]) \tag{3}$$

where Δt is the discretization step, and $[I]$ denotes an identity matrix. On the basis of (3), the discrete-time eigenvalues z_i from $[A_d]$ and continuous-time eigenvalues λ_i from $[A_c]$ can be converted to each other as (4).

$$\lambda_i = \frac{2}{\Delta t} \frac{z_i - 1}{z_i + 1} \quad or \quad z_i = \frac{2 + \Delta t \lambda_i}{2 - \Delta t \lambda_i} \tag{4}$$

It is well known that the system's small-signal stability is determined by the position of eigenvalues in the complex plane. Generally, the left half part in the s-plane is the stable region for continuous-time systems, while the unit circle in the z-plane is the stable region for discrete-time systems.

It should be clarified that the discrete-time state matrix $[A_d]$ in the general discrete-time method is obtained by discretizing the full-order continuous-time state matrix $[A_c]$. However, this paper is devoted to developing a more efficient method for constructing the state matrix directly within the discrete-time domain. This new method is suitable for the eigenvalue analysis of SSO in AC/DC hybrid power systems. In this context, the proposed method mainly consists of three steps: 1) establishing the discrete-time state-space model and its equivalent circuit of each component including their controller dynamics; 2) forming the discrete-time equivalent circuit of the whole system and applying the nodal analysis method to obtain the discrete-time state matrix; 3) solving the discrete-time eigenvalues and analyzing the stability of the target system. The following sections will introduce each step in detail.

III. Discrete-Time Models of AC/DC Components

A. A Conceptual AC/DC Hybrid Power System

Fig. 1 is a conceptual AC/DC hybrid system showing the main connection between the generation side, transmission side, and load side. In each part, some typical components are demonstrated as representatives. For example, the generation side includes various power generation components such as wind farms, photovoltaic stations, and synchronous generators. Electricity is generated and transmitted to the power load via transmission side components such as transformers, AC lines, and HVDC. In some cases, series-compensations and FACTS

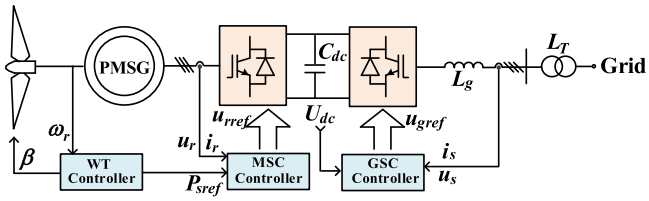

Fig. 2. Schematic diagram of PMSG.

are also adopted to improve the transmission capacity and stability in long-distance overhead lines. The problem of SSO is very common in such a structured power system according to engineering experiences.

For discrete-time eigenvalue analysis of this system, it is necessary to derive the DSSM and DECM of each component first. The following subsections will classify these involved components into three categories and establish their respective discrete-time models. It should be highlighted that the detailed controllers of those converter-based components are considered in the derived model.

B. Discrete-Time Model of Single-Port Component

The single-port components indicate those devices connected to the system by only one independent node. The permanent magnet synchronous generator (PMSG) exhibited in Fig. 2 is of this type. PMSG has a permanent magnet generator with its rotor mechanically driven by the wind turbine, and its stator is connected to the grid via a full-power back-to-back converter. A set of controllers are applied for efficient conversion of wind energy to power electricity while introducing complex dynamics such as SSO. This subsection takes the PMSG as an example to introduce the derivation of its discrete-time model.

The continuous-time state-space model of PMSG can be expressed as (5) [6]. It takes all its practical parts into account, including the mechanical components (shaft), the electrical components (permanent magnet generator, filter, and DC link), the full-scale control (PLL, inner & outer loops), and the time delay (measurement and pulse trigger).

$$p[X_s] = [A_{c-s}][X_s] + [B_{c-s}][U_{sxy}] \tag{5a}$$

$$[i_{sxy}] = [C_{c-s}][X_s] \tag{5b}$$

In the above equations, $[X_s]$ is the variation of the continuous-time state vector of PMSG; $[U_{sxy}]$ and $[i_{sxy}]$ are the variation of the input voltage and output current vector at the port in xy coordinate; $[A_{c\text{-}s}]$, $[B_{c\text{-}s}]$, and $[C_{c\text{-}s}]$ are coefficient matrices in the continuous-time domain; p is the differential operator.

Using the trapezoidal integration rule to discretize (5a), we can get:

$$[X_s(t)] = [A_s][U_{sxy}(t)] + [B_s][h_s(t)] \tag{6a}$$

$$[h_s(t)] = [C_s][U_{sxy}(t - \Delta t)] + [D_s][X_s(t - \Delta t)] \tag{6b}$$

Where $[h_s(t)]$ represents the term related to the previous time moment in the discretized expression, which is defined as the 'historical current term' (HCT) in this paper; $[A_s]$, $[B_s]$, $[C_s]$

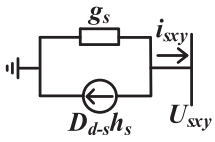

Fig. 3. Discrete-time equivalent circuit model of PMSG.

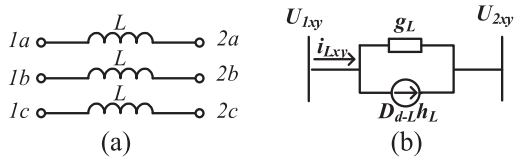

Fig. 4. Discrete-time equivalent circuit model of L branch.

and $[D_s]$ are coefficient matrices. To simplify the notation, let $a(t) = a$ and $a(t\text{-}\Delta t) = a$' in the following part.

Substituting (6a) into (6b) and (5b), the HCT iteration expression as well as the relationship between output current and HCT can be obtained:

$$[h_s] = [A_{d-s}][h'_s] + [B_{d-s}][U'_{sxy}] \tag{7a}$$

$$[i_{sxy}] = [C_{d-s}][U_{sxy}] - [D_{d-s}][h_s] \tag{7b}$$

Where:

$$\begin{cases} [A_{d-s}] = [D_s][B_s] \\ [B_{d-s}] = [C_s] + [D_s][A_s] \\ [C_{d-s}] = [C_{c-s}][A_s] \\ [D_{d-s}] = -[C_{c-s}][B_s] \end{cases} \tag{8}$$

Note that formulas (7) and (2) have the same form, it is reasonable to define (7) as the DSSM of PMSG. According to (7b), the DECM of PMSG can be represented as Norton branch, as shown in Fig. 3, which is composed of an equivalent conductance and a historical current source (HCS) in parallel.

The conductance in Fig. 3 is expressed as:

$$\mathbf{g_s} = -[C_{d-s}] \tag{9}$$

Although the principles and mathematical models of other single-port components, such as photovoltaic stations, turbine generators, and SVG/SVC, et al., are different from PMSG, their DSSMs and DECMs can also be derived using the same modeling process as that of the PMSG.

Besides, it should be noted that this modeling process is equally valid for any other implicit integration rule such as backward Euler. The only distinction is that the corresponding coefficient matrices might be different when the integration rule changes.

C. Discrete-Time Model of Two-Port AC Component

The two-port AC components mainly include transformers, overhead lines, and series compensation capacitors in the power network. Unlike single-port components, these devices are connected to the network by two independent nodes. Although various two-port AC components in power systems have different physical structures and operating characteristics, they can all be represented as series or parallel combinations of the lumped *RLC* circuits for SSO study. Hence, it is necessary to study the discrete-time model of the basic *R/L/C* branch.

This subsection takes the *L* branch as an example to introduce the derivation of its discrete-time model. The differential equations of the *L* branch shown in Fig. 4(a) in the *xy* synchronous rotating coordinate can be described as:

$$p\begin{bmatrix} i_{Lx} \\ i_{Ly} \end{bmatrix} = \begin{bmatrix} \omega_b/X_L & 0 \\ 0 & \omega_b/X_L \end{bmatrix}\begin{bmatrix} U_{Lx} \\ U_{Ly} \end{bmatrix} + \begin{bmatrix} 0 & \omega_b \\ -\omega_b & 0 \end{bmatrix}\begin{bmatrix} i_{Lx} \\ i_{Ly} \end{bmatrix} \tag{10}$$

or in compact notation:

$$p[i_{Lxy}] = [A_{c-L}][i_{Lxy}] + [B_{c-L}][U_{Lxy}] \tag{11}$$

where $[i_{Lxy}]$ and $[U_{Lxy}]$ are branch current and voltage vector respectively, ω_b is rated angular frequency, and X_L is reactance per unit value. $[A_{c\text{-}L}]$ and $[B_{c\text{-}L}]$ are coefficient matrices.

Applying the trapezoidal integration rule to discretize (11), the DSSM of *L* branch is obtained as (12), where $[h_L]$ denotes the HCT of *L* branch, and $[A_{d\text{-}L}]$, $[B_{d\text{-}L}]$, $[C_{d\text{-}L}]$, $[D_{d\text{-}L}]$ are coefficient matrices in discrete-time domain.

$$[h_L] = [A_{d-L}][h'_L] + [B_{d-L}][U'_{Lxy}] \tag{12a}$$

$$[i_{Lxy}] = [C_{d-L}][U_{Lxy}] + [D_{d-L}][h_L] \tag{12b}$$

According to (12b), the DECM of *L* element in the form of the Norton branch can be described as Fig. 4(b), where the equivalent conductance is:

$$\mathbf{g_L} = [C_{d-L}] \tag{13}$$

For the capacitance element, the derivation of its DSSM and DECM is similar to the above process. Only the subscript '*L*' needs to be replaced by '*C*.' The discrete-time model of resistance is the same as its continuous-time model.

With the DSSMs and DECMs of *R/L/C* elements obtained, the two-port AC components in the power system can directly use their combination when constructing the networked DECM and performing SSO analysis.

D. Discrete-Time Model of Two-Port HVDC Component

The HVDC is also a two-port component, which is connected to the AC grid by two nodes. However, its discrete-time model is quite different from that of the AC line or transformer, mainly because the HVDC has two converters with distinct controls, causing its two sides totally asymmetric. This subsection takes the VSC-HVDC shown in Fig. 5 as an example to illustrate the derivation of the discrete-time model of HVDC.

The continuous-time state-space model of VSC-HVDC can be expressed as (14) if taking the AC bus voltage and current on both sides as input and output variables. It is capable of representing dynamics of the electrical components like DC line & capacitors and equivalent impedance of connecting transformer, as well as the control of both converters including PLL, current and

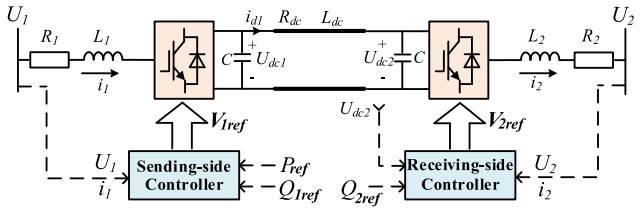

Fig. 5. Schematic diagram of VSC-HVDC.

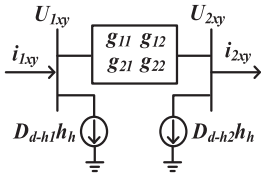

Fig. 6. Discrete-time equivalent circuit model of VSC-HVDC.

active/reactive power control loops.

$$p[X_h] = [A_{c-h}][X_h] + [B_{c-h1}][U_{1xy}] + [B_{c-h2}][U_{2xy}] \tag{14a}$$

$$[i_{1xy}] = [C_{c-h1}][X_h], \quad [i_{2xy}] = [C_{c-h2}][X_h] \tag{14b}$$

In (14), $[X_h]$ is the variation of the continuous-time state vector of VSC-HVDC; $[U_{1xy}]$ and $[U_{2xy}]$ are the variation of the input voltage vector at the bus in xy coordinate; $[i_{1xy}]$ and $[i_{2xy}]$ are the variation of the output current vector at AC side of converters in xy coordinate; $[A_{c\text{-}h}]$, $[B_{c\text{-}h1}]$, $[B_{c\text{-}h2}]$, $[C_{c\text{-}h1}]$ and $[C_{c\text{-}h2}]$ are coefficient matrices in continuous-time domain.

Using the trapezoidal integration rule to discretize (14a), the discretized equation and HCT of VSC-HVDC can be expressed as (15), where $[A_{h1}]$, $[A_{h2}]$, $[A_{h3}]$, $[B_{h1}]$, $[B_{h2}]$ and $[B_{h3}]$ are corresponding coefficient matrices.

$$[X_h] = [A_{h1}][h_h] + [A_{h2}][U_{1xy}] + [A_{h3}][U_{2xy}] \tag{15a}$$

$$[h_h] = [B_{h1}][X'_h] + [B_{h2}][U'_{1xy}] + [B_{h3}][U'_{2xy}] \tag{15b}$$

Substituting (15a) into (15b) and (14b), the DSSM of VSC-HVDC can be obtained as follows:

$$[h_h] = [A_{d-h}][h'_h] + [B_{d-h1}][U'_{1xy}] + [B_{d-h2}][U'_{2xy}] \tag{16a}$$

$$[i_{1xy}] = [C_{d-h1}][U_{1xy}] + [C_{d-h2}][U_{2xy}] + [D_{d-h1}][h_h] \tag{16b}$$

$$[i_{2xy}] = [C_{d-h3}][U_{1xy}] + [C_{d-h4}][U_{2xy}] - [D_{d-h2}][h_h] \tag{16c}$$

In (16), $[A_{d\text{-}h}]$, $[B_{d\text{-}h1}]$, $[B_{d\text{-}h2}]$, $[C_{d\text{-}h1}]$, $[C_{d\text{-}h2}]$, $[C_{d\text{-}h3}]$, $[C_{d\text{-}h4}]$, $[D_{d\text{-}h1}]$ and $[D_{d\text{-}h2}]$ are all coefficient matrices which can be calculated from coefficient matrices in (14) and (15).

According to (16b) and (16c), the DECM of VSC-HVDC can be described as Fig. 6, where $\boldsymbol{g}_{11}$ and $\boldsymbol{g}_{22}$ represent the respective self-conductance of the two bus nodes; $\boldsymbol{g}_{12}$ and $\boldsymbol{g}_{21}$ represent the mutual-conductance between the two side bus nodes. Note that, unlike the two-port AC component, the DECM of VSC-HVDC contains two different HCSs connected to sending and receiving side bus nodes, respectively.

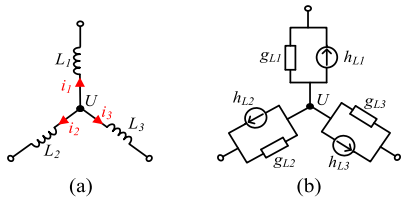

Fig. 7. Improper network of pure inductance cut-set and its equivalent circuit.

The conductance in Fig. 6 is expressed as:

$$\begin{cases} \mathbf{g_{11}} = [C_{d-h1}], & \mathbf{g_{12}} = -[C_{d-h2}] \\ \mathbf{g_{21}} = [C_{d-h3}], & \mathbf{g_{22}} = -[C_{d-h4}] \end{cases} \tag{17}$$

Note that the above modeling process can also be applied to LCC-HVDC and MMC-HVDC with related controls. All of their DSSMs and DECMs have the same form, while the specific coefficient matrices might be different.

IV. Discrete-time State-Space Construction of AC/DC Hybrid System

A. Determination of Discrete-Time State Variables

Theoretically, the selection of state variables is not unique, any set of n linearly independent variables may be used to describe the state of the system. Note that the expression of HCTs in the DSSMs of various components in Section III all have the same form as (2). Therefore, it is reasonable to select the HCTs as the discrete-time variables internal to components.

It is well known that the biggest inconvenience of the continuous-time state-space method is the requirements of topological analysis to find independent state variables for improper networks. Otherwise, it may be impossible to invert a non-full rank matrix in the process of intermediate variables elimination. For the single-phase pure inductance cut-set circuit shown in Fig. 7(a), the three branch currents have the relation of (18), and thus only two of them (e.g., i_2 and i_3) are independent in the continuous-time domain.

$$i_1 + i_2 + i_3 = 0 \tag{18}$$

When this typical improper network is described by the discrete-time model, its equivalent circuit is demonstrated as Fig. 7(b). To find the linear relation of the three discrete-time state variables h_{Li} (i = 1, 2, 3) related to this circuit, it is necessary to solve the coefficients k_j (j = 1, 2, 3) in (19).

$$k_1 h_{L1} + k_2 h_{L2} + k_3 h_{L3} = 0 \tag{19}$$

Simplifying (12) into an equation describing single-phase circuits, and then substituting this and (18) into (19) yields

$$M_1 U + M_2 i_2 + M_3 i_3 = 0 \tag{20}$$

where the coefficient expressions are as follows:

$$\begin{cases} M_1 = k_1 g_{L1} + k_2 g_{L2} + k_3 g_{L3} \\ M_2 = k_2 - k_1 \\ M_3 = k_3 - k_1 \end{cases} \tag{21}$$

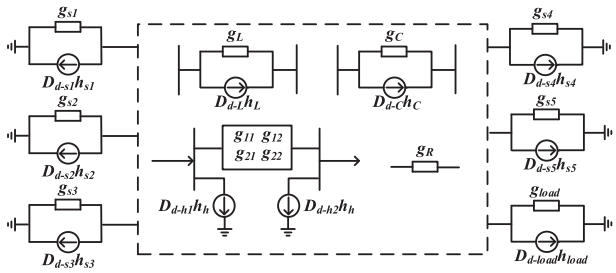

Fig. 8. The networked DECM of the conceptual AC/DC hybrid system.

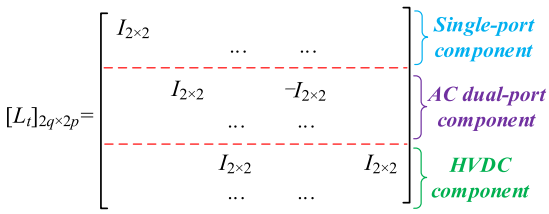

Fig. 9. Elements classification in branch-node incidence matrix.

Considering the linear independence relation between the currents i_2 and i_3 and the voltage U, the real coefficients M_i (i = 1, 2, 3) in (20) are all equal to zero. According to (21), it can be further calculated that $k_1 = k_2 = k_3 = 0$, thus proving that the three discrete-time state variables in Fig. 7 are linearly independent.

Here, it is found that the so-called improper network and the resulting independent state variables selection problem in the continuous-time domain will naturally disappear in the discrete-time domain, thus making the topology analysis unnecessary in the discrete-time method. Further analysis shows that the practice of combining currents and voltages as discrete-time state variables is the essential reason for these advantages.

Since [$h(t)$] can be expressed as a linear combination of [$h(t\text{-}\Delta t)$] and [$U(t\text{-}\Delta t)$], in order to generate the discrete-time state matrix of the entire system, it is necessary to eliminate the intermediate variables [$U(t\text{-}\Delta t)$].

B. Networked DECM of System and Its Nodal Description

With all components modeled as DECMs, the entire system can then be represented as a networked DECM by connecting all individual circuit models according to the system topology. For the conceptual AC/DC hybrid system, its networked DECM is shown in Fig. 8, which is composed of HCSs and equivalent conductance from different components.

For a system or networked DECM with p nodes and q branches, the node conductance matrix $[G]_{2p\times 2p}$ and the branch-node incidence matrix $[L_t]_{2q\times 2p}$ can be generated very easily. For the incidence matrix shown in Fig. 9, the elements corresponding to the single-port component node is set as identity matrix $I_{2\times 2}$ while the elements corresponding to the two-port AC component nodes are set as $I_{2\times 2}$ and $-I_{2\times 2}$, and elements corresponding to the HVDC nodes are $I_{2\times 2}$ and $I_{2\times 2}$. All other elements in the incidence matrix are set to 0.

In a networked DECM with arbitrary structure, its nodal equations can be described as:

$$[G][U_{node}] = [i_{inject}] \quad or \quad [U_{node}] = [G]^{-1}[i_{inject}] \tag{22}$$

where $[U_{node}]$ and $[i_{inject}]$ represent the column vector of node voltages and node injection currents, respectively.

According to the system's topology, the relationship between branch voltages and node voltages is obtained as:

$$[U_{branch}] = [L_t][U_{node}] \tag{23}$$

Besides, the node injection current in terms of the HCSs of individual components are given as:

$$[i_{inject}] = -[L_t]^T[HCS] \tag{24}$$

where the superscript 'T' denotes the transpose of the matrix.

C. Discrete-Time State-Space Construction of AC System

Consider an AC system without HVDC transmission first, which only consists of single-port and AC two-port components. For such a system, write the discrete-time state variables (HCTs) of all components in matrix form in order:

$$\begin{bmatrix} h_s \\ \cdots \\ h_{L/C} \\ \cdots \end{bmatrix} = \begin{bmatrix} A_{d-s} & 0 & 0 & 0 \\ 0 & \cdots & 0 & 0 \\ 0 & 0 & A_{d-L/C} & 0 \\ 0 & 0 & 0 & \cdots \end{bmatrix} \begin{bmatrix} h'_s \\ \cdots \\ h'_{L/C} \\ \cdots \end{bmatrix} + \begin{bmatrix} B_{d-s} & 0 & 0 & 0 \\ 0 & \cdots & 0 & 0 \\ 0 & 0 & B_{d-L/C} & 0 \\ 0 & 0 & 0 & \cdots \end{bmatrix} \begin{bmatrix} U'_{sxy} \\ \cdots \\ U'_{L/Cxy} \\ \cdots \end{bmatrix} \tag{25}$$

or, in compact notation

$$[h] = [A_d][h'] + [B_d][U'_{branch}] \tag{26}$$

Also, the relationship between HCSs in Fig. 8 and HCTs in DSSMs of components is given as:

$$\begin{bmatrix} HCS_s \\ \cdots \\ HCS_{L/C} \\ \cdots \end{bmatrix} = \begin{bmatrix} D_{d-s} & 0 & 0 & 0 \\ 0 & \cdots & 0 & 0 \\ 0 & 0 & D_{d-L/C} & 0 \\ 0 & 0 & 0 & \cdots \end{bmatrix} \begin{bmatrix} h_s \\ \cdots \\ h_{L/C} \\ \cdots \end{bmatrix} \tag{27}$$

or, in compact notation

$$[HCS] = [D_d][h] \tag{28}$$

Substituting (22), (23), (24), and (28) into (26), the iteration expression of [h(t)] with all intermediate variables eliminated can be obtained as:

$$[h] = [A_d][h'] + [B_d][L_t][G]^{-1}[-L_t]^T[D_d][h'] \tag{29}$$

Compared with the standard form of discrete-time state-space formulation (2) without forcing function ($u(t) = 0$), the discrete-time state matrix $[A_D]$ of the AC system is found as follows:

$$[A_D] = [A_d] + [B_d][L_t][G]^{-1}[-L_t]^T[D_d] \tag{30}$$

Some observations can be made regarding these matrices:

1) $[A_d]$, $[B_d]$ and $[D_d]$ are all diagonal matrices, and their diagonal elements are composed of the coefficient matrices in the DSSMs of each component;
2) $[G]$ is the node conductance matrix composed of equivalent conductance in the networked DECM of the system;
3) $[L_t]$ is a branch-node incidence matrix reflecting the system topology.

D. Discrete-Time State-Space Construction of AC/DC System

From (16), it can be seen that unlike the models of single-port and two-port AC components, there are two input voltages and two historical current sources in the discrete-time model of HVDC. The coefficient matrices $[B_{d\text{-}h1}]$, $[B_{d\text{-}h2}]$, $[D_{d\text{-}h1}]$, and $[D_{d\text{-}h2}]$ cannot be filled into the diagonal matrices $[B_d]$ and $[D_d]$ directly. Therefore, it is unable to directly obtain the state matrix of the AC/DC hybrid system based on (30).

Here, the matrix $[B_d]$ is taken as an example to briefly explain the defects. The input variables corresponding to $[B_d]$ in (26) represent the branch voltages of AC components. However, there is no actual concept of a branch voltage for HVDC, and the two input voltages in DSSM of HVDC in (16a) are all node voltages. Therefore, Eq. (30) cannot be used to uniformly eliminate all the voltage variables of different components in an AC/DC system.

As an alternative, considering that the term $([B_d][L_t])$ in (30) represents the process of transforming the branch voltages to the node voltages, it is feasible to find a way to eliminate the node voltage variables of HVDC after calculating '$[B_d][L_t]$.' The process of forming diagonal $[D_d]$ is similar to that of $[B_d]$.

For the convenience of the description below, it is assumed that the HVDC branch number is '*k*', the sending end AC bus node number is '*m*', and the receiving end AC bus node number is '*n*'. The process is explained as follows:

- Form the diagonal matrix $[A_d]$, branch-node incidence matrix $[L_t]$, and node conductance matrix $[G]$ in the same way as in the AC system;
- The diagonal element corresponding to branch *k* in $[B_d]$ and [Dd] is temporarily set by I2×2, while other diagonal elements are generated in the same way as in the AC system;
- Calculate separately: $([B_d][L_t] = [BL])$ and $(-[L_t]T\,[D_d] = [LD])$;
- Replace the elements at row (2*k*-1,2*k*) and column (2*m*-1,2*m*) in [BL] with $[B_d\text{-}h1]$, and the elements at row (2*k*-1,2*k*) and column (2*n*-1,2*n*) with $[B_d\text{-}h2]$;
- Replace the elements at row (2*m*-1,2*m*) and column (2*k*-1,2*k*) in [*LD*] with $[D_d\text{-}h1]$, and the elements at row (2*n*-1,2*n*) and column (2*k*-1,2*k*) with $[D_d\text{-}h2]$;

Then, the discrete-time state matrix $[A_D]$ of the AC/DC hybrid system is derived as (31), which is compatible with (30).

$$[A_D] = [A_d] + [BL][G]^{-1}[LD] \tag{31}$$

It can be seen that through the last two steps of matrix elements replacement processing, the problems of eliminating the two node voltages and two current sources in the discrete-time model of HVDC can be solved successfully.

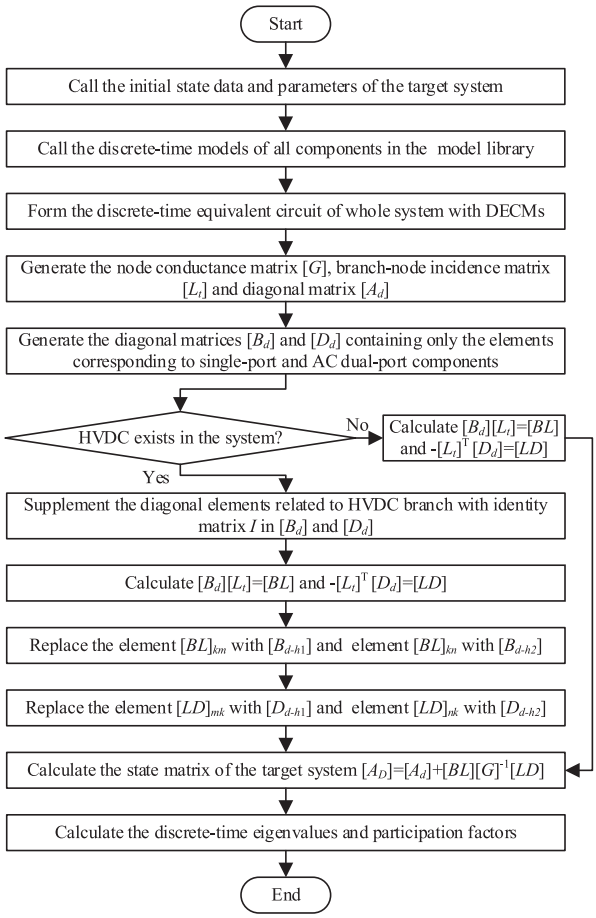

Fig. 10. Basic procedures of discrete-time eigenvalue analysis.

Based on the above contents, the procedures of the proposed discrete-time state-space construction method for complicated AC/DC hybrid systems with arbitrary structures can be concluded as Fig. 10. Furthermore, it must be pointed out that the discrete-time modeling method for various components and the state-space construction method for the whole AC/DC hybrid system proposed in this paper are also applicable to more complex systems that may include three-port or multi-port components like multi-terminal HVDC. However, due to space limitations and the uncommonness of these components, they will not be repeatedly introduced in detail here.

V. Case System Analysis and Verification

Three case systems are presented in this section to validate the proposed discrete-time state-space method. Among them, the first two simple case examples are respectively used to illustrate the realization process of (30) and (31), so as to facilitate readers to understand more intuitively. The third case focuses on the practicability and effectiveness of the proposed method in the practical complex AC/DC hybrid system. All of those analysis results are validated through electromagnetic transient simulations. It should be noted that in addition to these examples, the proposed method can also be used in any other SSO scenarios, as long as the target system can be linearized.

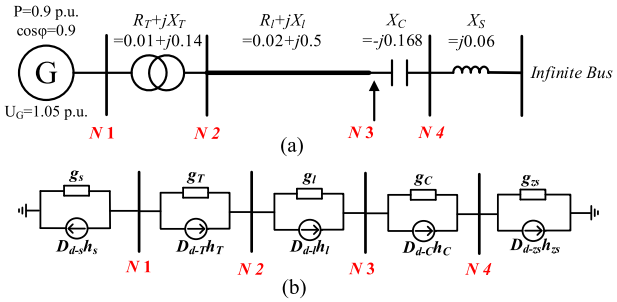

Fig. 11. IEEE first benchmark model: (a) structure diagram; (b) networked discrete-time equivalent circuit.

A. AC Case: IEEE First Benchmark Model

The structure diagram of the *IEEE first benchmark model* and its corresponding parameters for SSO analysis are shown in Fig. 11(a). It has 4 nodes and 5 branches. There are 5 natural torsional oscillation frequencies of the generator shaft system, which are 15.7Hz\20.2Hz\25.2Hz\32.3Hz\47.5Hz. The series compensation degree is 30% in the studied condition.

This case system consists of only single-port and two-port AC components. Based on the derived DSSMs and DECMs in Section III, the benchmark system is equivalent to the networked discrete-time circuit in Fig. 11(b), from which, the node conductance matrix and the branch-node incidence matrix can be easily obtained as (32). In addition, the diagonal matrices in (30) are expressed as (33).

$$\begin{cases} [G]=\begin{bmatrix} g_s+g_T & -g_T & 0_2 & 0_2 \\ -g_T & g_T+g_l & -g_l & 0_2 \\ 0_2 & -g_l & g_l+g_C & -g_C \\ 0_2 & 0_2 & -g_C & g_C+g_{zs} \end{bmatrix} \\ [L_t]=\begin{bmatrix} I_2 & 0_2 & 0_2 & 0_2 \\ I_2 & -I_2 & 0_2 & 0_2 \\ 0_2 & I_2 & -I_2 & 0_2 \\ 0_2 & 0_2 & I_2 & -I_2 \\ 0_2 & 0_2 & 0_2 & I_2 \end{bmatrix} \end{cases} \tag{32}$$

$$\begin{cases} [A_d]=\begin{bmatrix} A_{d-s} & & & \\ & A_{d-T} & 0 & \\ & & A_{d-l} & \\ & 0 & & A_{d-C} \\ & & & & A_{d-zs} \end{bmatrix} \\ [B_d]=\begin{bmatrix} B_{d-s} & & & \\ & B_{d-T} & 0 & \\ & & B_{d-l} & \\ & 0 & & B_{d-C} \\ & & & & B_{d-zs} \end{bmatrix} \\ [D_d]=\begin{bmatrix} D_{d-s} & & & \\ & D_{d-T} & 0 & \\ & & D_{d-l} & \\ & 0 & & D_{d-C} \\ & & & & D_{d-zs} \end{bmatrix} \end{cases} \tag{33}$$

TABLE I
NATURAL MODES OF IEEE FIRST BENCHMARK MODEL

Mode	Discrete-time Eigenvalues	Continuous-time Eigenvalues 1	Continuous-time Eigenvalues 2
$\lambda_{1,2}$	0.99998±j0.00496	-0.13718±j99.229	-0.13718±j99.229
$\lambda_{3,4}$	0.99995±j0.00635	-0.6527±j127.03	-0.6527±j127.03
$\lambda_{5,6}$	0.99996±j0.00803	-0.14785±j160.69	-0.14785±j160.69
$\lambda_{7,8}$	**0.99997±j0.01017**	**0.49044±j203.45**	**0.49044±j203.45**
$\lambda_{9,10}$	0.99988±j0.01491	-0.18179±j298.18	-0.18179±j298.18

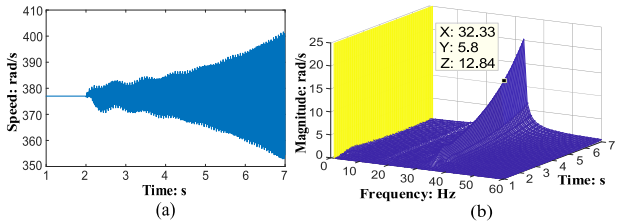

Fig. 12. Simulation results of IEEE first benchmark model: (a) generator speed; (b) spectrum of generator speed.

With the above coefficient matrices obtained, the discrete-time state matrix $[A_D]$ of the benchmark system is finally calculated based on Eq. (30). Table I lists the eigenvalues corresponding to the 5 shaft torsional modes, where the second column shows the results of the proposed discrete-time method. The third and fourth columns respectively denote continuous-time eigenvalues obtained through: i) the conversion from discrete-time eigenvalues using (4), and ii) the conventional continuous-time state-space method. It can be found that the eigenvalues from different methods are exactly consistent, which validates the correctness of the proposed discrete-time method.

Moreover, it is notable that the continuous-time eigenvalues in the third column converted by (4) are independent of the chosen integration step Δt, since the mapping of the discrete-time eigenvalues into the continuous-time ones reverses the distortion error induced by the discretization process of the state-space model [43]. Theoretically, as long as the maximum mode frequency of the system is below the Nyquist frequency defined by $f_{Ny} = 1/(2\Delta t)$, the corresponding eigenvalue results can be correctly computed.

Some time-domain simulations of the benchmark system are performed in PSCAD/EMTDC. Under the aforementioned system operating condition, the generator speed waveform and its spectrum analysis results are shown in Fig. 12. It is observed that the generator speed diverges rapidly after disturbance and the major oscillation frequency is also consistent with the unstable mode in Table I, thus verifying the proposed method again.

B. HVDC Case: Two-Terminal VSC-HVDC System

The two-terminal VSC-HVDC case example shown in Fig. 13(a) is used to illustrate the process of generating the discrete-time state matrix of a system containing HVDC. Its networked DECM is given as Fig. 13(b), which also has 4 nodes and 5 branches.

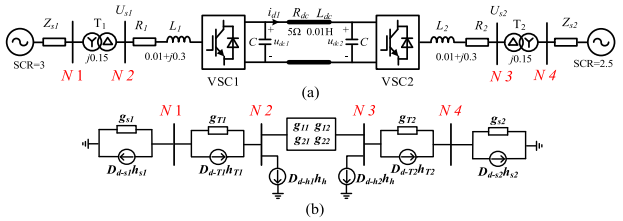

Fig. 13. Two-terminal VSC-HVDC system: (a) structure diagram; (b) networked discrete-time equivalent circuit.

The node conductance matrix and the branch-node incidence matrix of such a system are obtained as (34).

$$\begin{cases} [G]=\begin{bmatrix} g_{s1}+g_{T1} & -g_{T1} & 0_2 & 0_2 \\ -g_{T1} & g_{T1}+g_{11} & -g_{12} & 0_2 \\ 0_2 & -g_{21} & g_{22}+g_{T2} & -g_{T2} \\ 0_2 & 0_2 & -g_{T2} & g_{T2}+g_{s2} \end{bmatrix} \\ [L_t]=\begin{bmatrix} I_2 & 0_2 & 0_2 & 0_2 \\ 0_2 & 0_2 & 0_2 & I_2 \\ I_2 & -I_2 & 0_2 & 0_2 \\ 0_2 & 0_2 & I_2 & -I_2 \\ 0_2 & I_2 & I_2 & 0_2 \end{bmatrix} \end{cases} \tag{34}$$

Besides, based on the steps described in the previous section, the three diagonal matrices are temporarily expressed as (35).

$$\begin{cases} [A_d]=\begin{bmatrix} A_{d-s1} & & & & \\ & A_{d-s2} & & 0 & \\ & & A_{d-T1} & & \\ & 0 & & A_{d-T2} & \\ & & & & A_{d-h} \end{bmatrix} \\ [B_d]=\begin{bmatrix} B_{d-s1} & & & & \\ & B_{d-s2} & & 0 & \\ & & B_{d-T1} & & \\ & 0 & & B_{d-T2} & \\ & & & & I_2 \end{bmatrix} \\ [D_d]=\begin{bmatrix} D_{d-s1} & & & & \\ & D_{d-s2} & & 0 & \\ & & D_{d-T1} & & \\ & 0 & & D_{d-T2} & \\ & & & & I_2 \end{bmatrix} \end{cases} \tag{35}$$

Then, matrices [*BL*] and [*LD*] are calculated as (36).

$$\begin{cases} [BL]=[B_d][L_t] \\ \quad =\begin{bmatrix} B_{d-s1} & 0 & 0 & 0 \\ 0 & 0 & 0 & B_{d-s2} \\ B_{d-T1} & -B_{d-T1} & 0 & 0 \\ 0 & 0 & B_{d-T2} & -B_{d-T2} \\ 0 & I_2([B_{d-h1}]) & I_2([B_{d-h2}]) & 0 \end{bmatrix} \\ [LD]=-[L_t]^T[D_d] \\ \quad =\begin{bmatrix} -D_{d-s1} & 0 & -D_{d-T1} & 0 & 0 \\ 0 & 0 & D_{d-T1} & 0 & -I_2([D_{d-h1}]) \\ 0 & 0 & 0 & -D_{d-T2} & -I_2([D_{d-h2}]) \\ 0 & -D_{d-s2} & 0 & D_{d-T2} & 0 \end{bmatrix} \end{cases} \tag{36}$$

TABLE II
NATURAL MODES OF TWO-TERMINAL VSC-HVDC SYSTEM

Mode	Discrete-time Eigenvalues	Continuous-time Eigenvalues 1	Continuous-time Eigenvalues 2
$\lambda_{1,2}$	0.99885±j0.0009	-22.91±j17.73	-22.91±j17.73
$\lambda_{3,4}$	**1.0003±j0.00357**	**6.291±j71.44**	**6.291±j71.44**
$\lambda_{5,6}$	0.9759±j0.00809	-487.7±j165.75	-487.7±j165.75
$\lambda_{7,8}$	0.9922±j0.0201	-152.4±j405.27	-152.4±j405.27
$\lambda_{9,10}$	0.9877±j0.02903	-238.3±j587.48	-238.3±j587.48

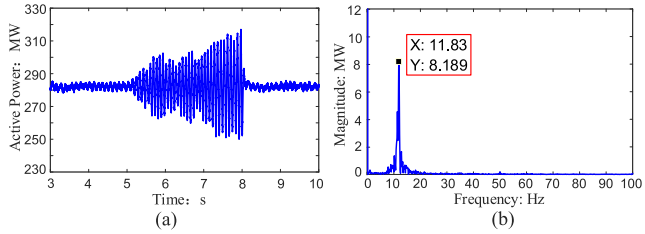

Fig. 14. Simulation results of two-terminal VSC-HVDC system: (a) active power; (b) spectrum of active power.

Further, replace the two red identity matrices in the last row of [*BL*] with [$B_{d\text{-}h1}$] and [$B_{d\text{-}h2}$] in the HVDC model, and similarly replace the red elements in the last column of [*LD*] with [$D_{d\text{-}h1}$] and [$D_{d\text{-}h2}$]. So far, all the required coefficient matrices have been obtained, and finally, the discrete-time state matrix can be calculated using (31).

Table II lists part of the eigenvalue results of this simple case system. It is seen that eigenvalues from the traditional continuous-time method and the novel discrete-time method are still consistent. The time-domain simulation results in Fig. 14 also show that oscillation frequency is almost the same as the calculated unstable mode. Thus, both of them prove the correctness of the proposed method, especially the formula (31).

C. Practical AC/DC Hybrid Case System

1) Target System Introduction: The structure diagram of the AC/DC hybrid system adapted from a practical system located in northwestern China is illustrated in Fig. 15. It contains four wind farms and two thermal power plants. Part of the generated power is sent to the local main grid through 750kV AC lines, and the other part is transmitted to the Central China Power Grid through the ±800kV HVDC transmission line. In 2015, a severe SSO induced by these PMSG-based wind farms excited the torsional oscillation on shafts of the units in Plant 1, causing three units tripped by TSR. Afterward, the researchers carried out lots of investigation and research on the accident, and also achieved some meaningful results, but there was almost no report on eigenvalue analysis for SSO of such a complex AC/DC hybrid system. This paper intends to use this system to further prove the applicability and effectiveness of the proposed method in practical complex power systems.

2) Discrete-Time Eigenvalue Analysis: According to the DSSMs and DECMs of various components and the procedures

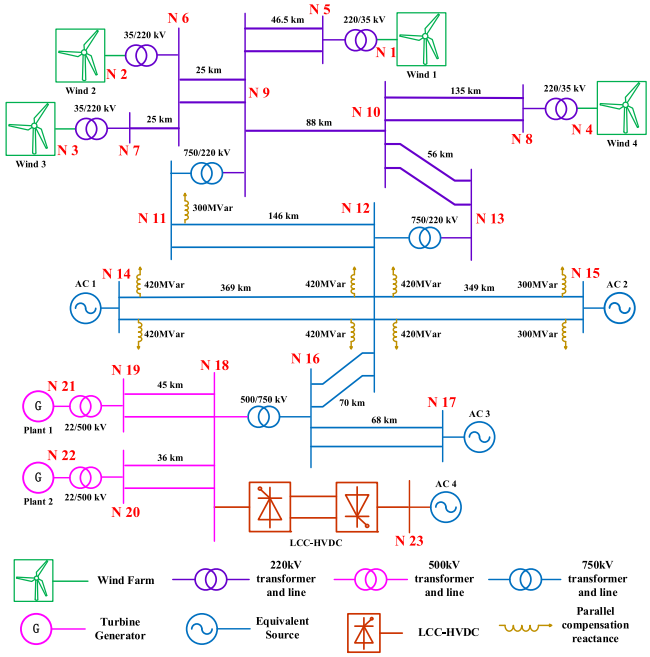

Fig. 15. Structure diagram of the adapted AC/DC hybrid system with RPG.

TABLE III
STEADY-STATE POWER FLOW OF TARGET AC/DC SYSTEM

Nodes	P(MW), Q(MVar)	Nodes	P(MW), Q(MVar)
N1→N5	399.9, 7.8	N12→N15	1736.8, -186.4
N2→N6	201.2, 2.5	N14→N0	-2750, 156
N3→N7	100.6, 1.63	N15→N0	1724, 190.3
N4→N8	99.8, 1.22	N12→N16	1750.6, -310.9
N9→N10	38.7, -24.7	N17→N0	652.6, 206.3
N10→N13	133.1, 45.8	N18→N16	-1095, 255.7
N11→N12	638.4, 183.7	N21→N19	1778, 182
N13→N12	133.3, 61.2	N22→N20	1146, 157.6
N12→N14	-2722, 248.4	N18→HVDC	4016, -148.3

TABLE IV
DOMINANT EIGENVALUES OF TARGET AC/DC SYSTEM

Mode	Discrete-time Eigenvalues	Continuous-time Eigenvalues	Oscillation Frequency (Hz)	Damping Ratio (1/s)
$\lambda_{91,92}$	0.9977±j0.0375	-31.97±j752.4	119.75	0.0425
$\lambda_{99,100}$	0.9977±j0.022	-41.05±j441.5	70.26	0.0926
$\lambda_{105,106}$	0.9993±j0.0181	-10.48±j362.33	57.67	0.0289
$\lambda_{111,112}$	**1.0008±j0.008667**	**17.034±j173.2**	**27.566**	**-0.0979**
$\lambda_{113,114}$	0.9999±j0.0082	-0.0258±j164.96	26.25	0.0002
$\lambda_{135,136}$	0.99998±j0.0051	-0.1479±j101.11	16.09	0.0015
$\lambda_{153,154}$	0.9994±j0.002	-12.95±j40.36	6.424	0.3055
$\lambda_{175,176}$	0.9999±j0.0007	-0.6422±j13.4	2.133	0.0479

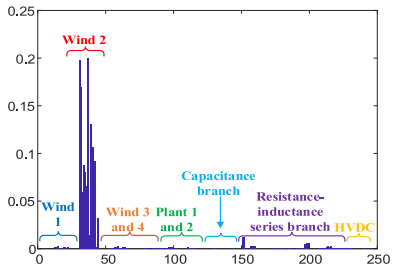

Fig. 16. Participation factors of the dominant eigenvalue.

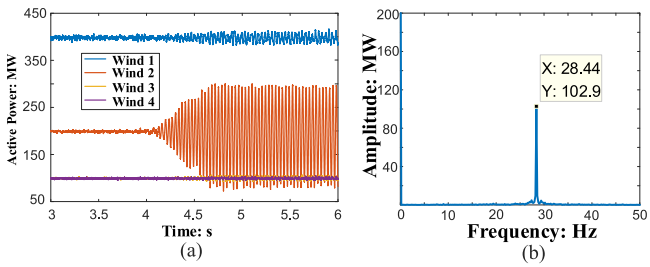

Fig. 17. (a) Active power in four wind farms; (b) spectrum of active power in wind farm 2.

in Fig. 10, a set of discrete-time eigenvalue analysis programs was developed based on MATLAB. The program can quickly generate the discrete-time state matrix after inputting the initial parameters and calculate the discrete-time eigenvalues as well as drawing a histogram of the participation factors of the dominant unstable mode.

It is assumed that the wind farms in the target system are simulated by multiple wind turbines with the same type and parameters, and the transmission lines are represented by π-type branches with lumped parameters. Under this circumstance, the total order of this case system is 245. Compared with the continuous-time method, it is easier to form the state matrix and perform eigenvalue analysis for such a system directly with the prepared program. The power flow under the steady-state operating point is demonstrated in Table III, and Table IV lists part of the eigenvalues of the target system calculated by the program. It can be seen that there is a dominant discrete-time eigenvalue with its absolute value greater than 1, indicating its instability. The continuous-time eigenvalue converted from the discrete-time shows that the oscillation frequency and damping ratio related to the unstable mode are 27.566Hz and -0.0979.

The participation factor of the unstable mode is shown in Fig. 16. It can be seen that this unstable mode is mainly related to the state variables in wind farm 2, and the participation of other parts of the system is almost negligible.

3) Simulation Validation: The detailed electromagnetic transient simulation model of the AC/DC hybrid system shown in Fig. 15 is constructed in PSCAD/ EMTDC. Fig. 17(a) shows the active power generated by the four wind farms. In the simulation, the proportional gain of the inner current control loop of wind turbine generators in wind farm 2 is changed from 1.2 to 0.3 at 4s, while the parameters in other wind farms remain unchanged. This setting is the same as the conditions in eigenvalue analysis. The Fourier decomposition result of active power is given in Fig. 17(b).

It can be seen that with low inner current control bandwidth, an apparent power oscillation occurs in wind farm 2, and the oscillation frequency is 28.44Hz. The other three wind farms have only a small amount of oscillation components, which is believed to be induced by wind farm 2. The error between the simulation result and the calculated discrete-time eigenvalue is 3.17%, thus validating the practicability of the proposed discrete-time eigenvalue method in large-scale AC/DC hybrid systems. The main reason for this frequency error is that the eigenvalues only reflect the small-signal stability of the equilibrium point. But in the simulation, as the oscillation diverges and reaches the constant amplitude region, it has slightly deviated from the original steady-state operating point.

Besides, in order to further verify the advantages of the proposed method in the application under the system's structure changes, one more simulation and eigenvalue analysis results will be given in the Appendix.

VI. Discussion on the Proposed Method

Considering that the focus of this paper is to propose a new approach for SSO analysis, this section aims to discuss the advantages and differences between it and other typical SSO analysis methods such as the continuous-time state-space method and the frequency-domain impedance method. This type of comparison could help readers to have a comprehensive understanding of various analysis methods and choose the appropriate one in practical applications.

A. Advantages Over the Continuous-Time State-Space Method

As an alternative to the conventional continuous-time state-space method, the proposed discrete-time state-space method has the ability to handle complex converter-based power systems with large-scale renewables and HVDC integrated, due to its great advantage of avoiding the topology analysis process.

In the application of conventional continuous-time method in complex systems, it is necessary to firstly perform topology analysis on the target system to find the network proper tree and then determine the independent state variables. When this is done, there is another difficulty to combine the models of individual components into the system-level model due to the extensive couplings among the state variables. Usually, a large number of complicated and irregular algebraic operations are required. Unfortunately, the previous process needs to be repeated when the structure of the system changes. It is for these reasons that there are few practical applications of the conventional continuous-time state-space method in large-scale complex power systems.

However, the proposed discrete-time state-space method can completely avoid the topology analysis. Since the target system is represented as a networked DECM, and the historic current terms of components are selected as the discrete-time state variables, the system-level model is only a straightforward interconnection of components' DSSMs according to the basic theory of nodal analysis. Moreover, the coefficient matrices used to generate the discrete-time state matrix are all diagonal matrices, thus making it possible to directly add or delete the corresponding diagonal elements to solve for the new state matrix when the system structure changes.

B. Differences From Frequency-Domain Impedance Method

The proposed discrete-time state-space method can retain the topology information of the target system by constructing the networked DECM, which has similar features as the impedance method in [35]. However, there are some obvious differences between these two methods in the following aspects:

1) System Representation: In the impedance method, the components are represented as frequency-domain input-output impedance models (IMs), which are then interconnected to form the networked IM. However, in the proposed method, the target system is represented as a time-domain circuit, which is composed of equivalent conductance and current source.
2) Goal of Modeling: The goal of the impedance method is to aggregate all the individual IMs into a total lumped impedance according to a certain path, while the ultimate goal of the proposed method is to obtain the state matrix of the target system efficiently, which can be realized by adopting the node method.
3) Stability Criterion: As mentioned in the previous sections, the proposed method judges the stability of the target system by the position of the discrete-time eigenvalues on the z-plane. But in the impedance method, the system stability depends on the resistance value at the zero-crossing point of the reactance in the lumped impedance curves.

Despite the above differences, both the discrete-time state-space method and frequency domain impedance method have the potential for SSO analysis in practical large power systems with renewable generation integrated.

However, in actual applications, it must be pointed out that the deficiencies of the impedance network method are that it can only provide information of the unstable modes and cannot quantitatively analyze the influence of control parameters on the system stability. But these shortcomings can be overcome by the participation factor and parameter sensitivity analysis in the proposed discrete-time state-space method.

VII. Conclusion and Future Work

A novel state-space construction method within the discrete-time domain for complex AC/DC hybrid systems was presented in this paper. It could be identified as the development of eigenvalue analysis for the SSO study. In this new approach, the components in the power system were divided into three categories, namely single-port components, two-port AC components, and two-port HVDC components, the DSSMs and DECMs of which were derived respectively. By representing the entire system as a networked discrete-time equivalent circuit, the nodal equations were adopted to describe the target system. Based on this, the algorithms for quickly generating the discrete-time state matrix of any structural system were proposed. The discrete-time eigenvalue analysis was performed on IEEE first benchmark model,

two-terminal VSC-HVDC system, and a complex AC/DC hybrid system, and the analysis results are verified by time-domain simulation.

The significant features of the proposed discrete-time method are concluded as follows:

1) The established discrete-time models cover most of the components including their controllers' dynamics in the practical power system, which is the basis for studying SSO of converter-based AC/DC hybrid systems.
2) The discrete-time equivalent circuit of the whole system is proved to be a proper network, thus making it unnecessary to perform topology analysis for the target system to find the independent state variables, which saves a lot of time and effort.
3) The coefficient matrices used to calculate the system state matrix are mostly block-diagonal matrices, which are very easy to generate and modify programmatically in case the system structure changes.
4) The discrete-time models of components are modular, and the system is described by nodal equations, making this method promising to be embedded in EMTP.

Future works will be devoted to investigating the propagation path of oscillations in the system. Since the state-space construction method in this paper retains the structural information of the target system, it is expected to find out the distribution of the oscillating mode in all branches and nodes.

APPENDIX

The working condition of the AC/DC hybrid system case in Section V is that all the components in the system are put into operation. In order to further confirm the effectiveness and advantages of the proposed method, the results of one more case after the system structure is changed are supplemented here.

Under the new operating condition, the wind farm 4, the transformer and transmission lines between node 4 and node 10 are entirely disconnected, and thus the total state-space order of the case is decreased to 213. As a disturbance, the proportional gain of the inner current control loop of wind turbine generators in wind farm 3 is changed from 1.2 to 0.3 at 4s. For such a new system structure, when adopting the continuous-time state-space method, it needs to re-perform topology analysis for the system to find the new proper tree and independent state variables, and then conduct the complicated algebraic variables elimination operation. However, with the discrete-time state-space method in this paper, it is only necessary to modify the diagonal elements in the coefficient matrices and the elements corresponding to the relevant nodes in the node conductance matrix after importing the updated initial data in the program. The repeated topology analysis in the continuous-time state-space method is unnecessary here.

The dominant discrete-time eigenvalue on the above working condition is $\lambda_{97,98}=1.0017\pm$ j0.009176, and the corresponding continuous-time value is $34.908\pm$j$29.157\times 2\pi$. The participation factor analysis results shown in Fig. 18 indicate that this unstable mode is mainly caused by wind farm 3. The simulation results in Fig. 19 validate the eigenvalue results and also prove the advantages of the proposed method.

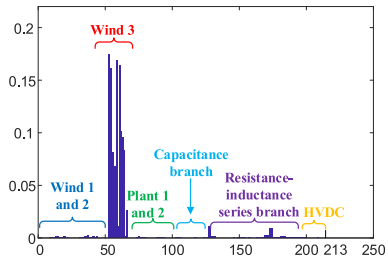

Fig. 18. Participation factors of the dominant eigenvalue under the new condition.

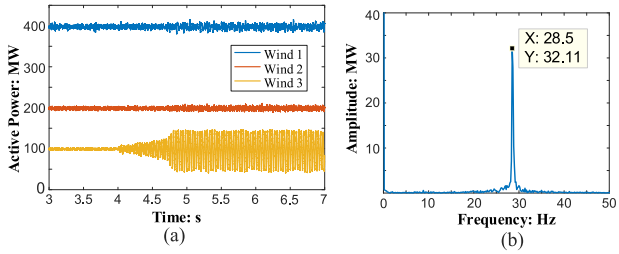

Fig. 19. Simulation results under the new condition: (a) active power in three wind farms; (b) spectrum of active power in wind farm 3.

REFERENCES

[1] Y. Li, L. Fan, and Z. Miao, "Wind in weak grids: Low-frequency oscillations, subsynchronous oscillations, and torsional interactions," *IEEE Trans. Power Syst.*, vol. 35, no. 1, pp. 109–118, Jan. 2020.
[2] M. Zhao, X. Yuan, J. Hu, and Y. Yan, "Voltage dynamics of current control time-scale in a VSC-connected weak grid," *IEEE Trans. Power Syst.*, vol. 31, no. 4, pp. 2925–2937, Jul. 2016.
[3] H. Liu *et al.*, "Subsynchronous interaction between direct-drive PMSG based wind farms and weak AC networks," *IEEE Trans. Power Syst.*, vol. 32, no. 6, pp. 4708–4720, Nov. 2017.
[4] X. Zhu, H. Sun, J. Wen, and S. Cheng, "Improved complex torque coefficient method using CPCM for multi-machine system SSR analysis," *IEEE Trans. Power Syst.*, vol. 29, no. 5, pp. 2060–2068, Sep. 2014.
[5] Subsynchronous Resonance Working Group of the System Dynamic Performance Subcommittee, "Reader's guide to subsynchronous resonance," *IEEE Trans. Power Syst.*, vol. 7, no. 1, pp. 150–157, Feb. 1992.
[6] B. Huang, H. Sun, Y. Liu, and L. Wang, "Study on subsynchronous oscillation in D-PMSGs-based wind farm integrated to power system," *IET Renew. Power Gener.*, vol. 13, no. 1, pp. 16–26, Jan. 2019.
[7] L. Xie *et al.*, "Wind integration in power systems: Operational challenges and possible solutions," *Proc. IEEE.*, vol. 99, no. 1, pp. 214–232, Jan. 2011.
[8] C. Zou *et al.*, "Analysis of resonance between a VSC-HVDC converter and the AC grid," *IEEE Trans. Power Electron.*, vol. 33, no. 12, pp. 10157–10168, Dec. 2018.
[9] S. H. Huang and Y. Gong, "South texas SSR," in *Proc. ERCOT ROS Meeting*, Austin, TX, USA, May 2018. [Online]. Available: http://www.ercot.com/content/wcm/key_documents_lists/139265/10._South_Texas_SSR_ERCOT_ROS_May_2018_rev1.pdf
[10] Y. Li, L. Fan, and Z. Miao, "Replicating real-world wind farm SSR events," *IEEE Trans. Power Del.*, vol. 35, no. 1, pp. 339–348, Feb. 2020.
[11] Y. Li, Y. Sun, H. Wang, F. Xing, and Z. Xu, "Sub- and super-synchronous oscillation analysis of hami renewable energy bases in xinjiang power grid," in *Proc. IEEE PES Asia-Pacific Power Energy Eng. Conf.*, 2019, pp. 1–5.
[12] L. Wang, X. Xie, Q. Jiang, H. Liu, Y. Li, and H. Liu, "Investigation of SSR in practical DFIG-based wind farms connected to a series-compensated power system," *IEEE Trans. Power Syst.*, vol. 30, no. 5, pp. 2772–2779, Sep. 2015.

[13] H. Liu, X. Xie, C. Zhang, Y. Li, H. Liu, and Y. Hu, "Quantitative SSR analysis of series-compensated DFIG-based wind farms using aggregated *RLC* circuit model," *IEEE Trans. Power Syst.*, vol. 32, no. 1, pp. 474–483, Jan. 2017.

[14] J. Shair, X. Xie, L. Wang, W. Liu, J. He, and H. Liu, "Overview of emerging subsynchronous oscillations in practical wind power systems," *Renew. Sustain. Energy Rev.*, vol. 99, pp. 159–168, Jan. 2019.

[15] Y. Chi *et al.*, "Overview of mechanism and mitigation measures on multi-frequency oscillation caused by large-scale integration of wind power," *CSEE J. Power Energy Syst.*, vol. 5, no. 4, pp. 433–443, Dec. 2019.

[16] H. Liu *et al.*, "Subsynchronous interaction between direct-drive PMSG based wind farms and weak AC networks," *IEEE Trans. Power Syst.*, vol. 32, no. 6, pp. 4708–4720, Nov. 2017.

[17] J. Lyu *et al.*, "Sub-synchronous oscillation mechanism and its suppression in MMC-based HVDC connected wind farms," *IET Gener. Trans. Distr.*, vol. 12, no. 4, pp. 1021–1029, Feb. 2018.

[18] B. Shao, S. Zhao, Y. Yang, B. Gao, and F. Blaabjerg, "Sub-synchronous oscillation characteristics and analysis of direct-drive wind farms with VSC-HVDC systems," *IEEE Trans. Sustain. Energy*, vol. 12, no. 2, pp. 1127–1140, Apr. 2021.

[19] M. Wu, R. Sun, L. Cheng, and L. Xie, "Parameter sensitivity analysis for sub-sybchronous control interactions in wind-integrated power systems," in *Proc. CIGRE Grid Future Symp.*, Houston, TX, USA, 2014, pp. 1–15.

[20] X. Xie, X. Zhang, H. Liu, Y. Li, and C. Zhang, "Characteristic analysis of subsynchronous resonance in practical wind farms connected to series-compensated transmissions," *IEEE Trans. Energy Convers.*, vol. 32, no. 3, pp. 1117–1126, Sep. 2017.

[21] B. Huang *et al.*, "Investigation on SSCI between PMSGs-based wind farm and AC network," *IET Renew. Power Gener.*, vol. 13, no. 16, pp. 2958–2965, Dec. 2019.

[22] L. Zhu, D. Zhong, B. Wang, R. Lin, and M. Xu, "Understanding sub-synchronous oscillation in DFIG-based wind farms with rotor-side converter control based on the equivalent RLC model," *IEEE Access*, vol. 8, pp. 65371–65382, 2020.

[23] Y. Xu, M. Zhang, L. Fan, and Z. Miao, "Small-signal stability analysis of type-4 wind in series-compensated networks," *IEEE Trans. Energy Convers.*, vol. 35, no. 1, pp. 529–538, Mar. 2018.

[24] J. Z. Zhou, H. Ding, S. Fan, Y. Zhang, and A. M. Gole, "Impact of short-circuit ratio and phase-locked-loop parameters on the small-signal behavior of a VSC-HVDC converter," *IEEE Trans. Power Deliv.*, vol. 29, no. 5, pp. 2287–2296, Oct. 2014.

[25] W. Dong, H. Xin, D. Wu, and L. Huang, "Small signal stability analysis of multi-infeed power electronic systems based on grid strength assessment," *IEEE Trans. Power Syst.*, vol. 34, no. 2, pp. 1393–1403, Mar. 2019.

[26] M. Amin and M. Molinas, "Small-signal stability assessment of power electronics-based power systems: A discussion of impedance- and eigenvalue- based methods," *IEEE Trans. Ind. Appl.*, vol. 53, no. 5, pp. 5014–5030, Sep./Oct. 2017.

[27] L. P. Kunjumuhammed, B. C. Pal, R. Gupta, and K. J. Dyke, "Stability analysis of a PMSG-based large offshore wind farm connected to a VSC-HVDC," *IEEE Trans. Energy Convers.*, vol. 32, no. 3, pp. 1166–1176, Sep. 2017.

[28] L. Shuai *et al.*, "Eigenvalue-based stability analysis of subsynchronous oscillation in an offshore wind power plant," in *Proc. 17th Int. Workshop Large-Scale Integration Wind Power into Power Syst. Well Transmiss. Netw. Offshore Wind Power Plants*, Stockholm, Sweden, 2018, pp. 1–5.

[29] J. Lyu, X. Cai, and M. Molinas, "Frequency domain stability analysis of MMC-based HVDC for wind farm integration," *IEEE J. Emerg. Sel. Top. Power Electron.*, vol. 4, no. 1, pp. 141–151, Mar. 2016.

[30] C. Zhang, X. Cai, M. Molinas, and A. Rygg, "On the impedance modeling and equivalence of AC/DC-side stability analysis of a grid-tied type-IV wind turbine system," *IEEE Trans. Energy Convers.*, vol. 34, no. 2, pp. 1000–1009, Jun. 2019.

[31] W. Du, C. Chen, and H. Wang, "Subsynchronous interactions induced by DFIGs in power systems without series compensated lines," *IEEE Trans. Sustain. Energy.*, vol. 9, no. 3, pp. 1275–1284, Jul. 2018.

[32] Y. Wang, J. Meng, X. Zhang, and L. Xu, "Control of PMSG-based wind turbines for system inertial response and power oscillation damping," *IEEE Trans. Sustain. Energy*, vol. 6, no. 2, pp. 565–574, Apr. 2015.

[33] W. Du, Q. Fu, H. Wang, and Y. Wang, "Concept of modal repulsion for examining the subsynchronous oscillations caused by wind farms in power systems," *IEEE Trans. Power Syst.*, vol. 34, no. 1, pp. 518–526, Jan. 2019.

[34] M. Zhao, X. Yuan, and J. Hu, "Modeling of DFIG wind turbine based on internal voltage motion equation in power systems phase-amplitude dynamics analysis," *IEEE Trans. Power Syst.*, vol. 33, no. 2, pp. 1484–1495, Mar. 2018.

[35] X. Xie, H. Liu, J. He, and W. Liu, "Small-signal impedance/admittance network modeling for grid-connected renewable energy generation systems," *Automat. Electric Power Syst.*, vol. 41, no. 12, pp. 26–32, Jun. 2017.

[36] W. Du, B. Ren, H. Wang, and Y. Wang, "Comparison of methods to examine sub-synchronous oscillations caused by grid-connected wind turbine generators," *IEEE Trans. Power Syst.*, vol. 34, no. 6, pp. 4931–4943, Nov. 2019.

[37] Z. Yang, C. Mei, S. Cheng, and M. Zhan, "Comparison of impedance model and amplitude-phase model for power-electronics-based power system," *IEEE J. Emerg. Sel. Top. Power Electron.*, vol. 8, no. 3, pp. 2546–2558, Sep. 2020.

[38] M. Parniani and M. R. Iravani, "Computer analysis of small-signal stability of power systems including network dynamics," *IEE Proc. Gener. Transmiss. Distrib.*, vol. 142, no. 6, pp. 613–617, Nov. 1995.

[39] P. M. Anderson, B. L. Agrawal, and J. E. Vaness, "Subsynchronous resonance in power systems," New York, NY, USA: Wiley-IEEE Press, 1990, pp. 93–105.

[40] E. S. Kun and R. A. Rohrer, "The state-variable approach to network analysis," *Proc. IEEE*, vol. 53, no. 7, pp. 672–686, Jul. 1965.

[41] X. Zhu, H. Sun, J. Wen, and S. Cheng, "A practical method to construct network state equations in multi-machine system SSR study," *Electric Power Syst. Res.*, vol. 107, pp. 51–58, 2014.

[42] K. Ogata, *Discrete-Time Control Systems*. Hoboken, NJ, USA: Prentice-Hall, 1994, pp. 321–312.

[43] J. A. Hollman and J. R. Marti, "Step-by-step eigenvalue analysis with EMTP discrete-time solutions," *IEEE Trans. Power Syst.*, vol. 25, no. 3, pp. 1220–1231, Aug. 2010.